A novel electrochemical biosensor with molecularly imprinted polymers and aptamer-based sandwich assay for determining amyloid-β oligomer

Min You, Shuai Yang, Yu An, Fan Zhang *, Pingang He

School of Chemistry and Molecular Engineering, East China Normal University, 500 Dongchuan Road, Shanghai 200241, PR China

ARTICLE INFO

ABSTRACT

Amyloid-β oligomers (AβOs) are highly toxic species involved in Alzheimer's disease (AD). Hence, a reliable detection method for AβOs, which are promising potential therapeutic targets and biomarkers for AD, is of great significance for improving the diagnosis of AD. Herein, a novel sandwich assay electrochemical biosensor was developed for highly sensitive and selective detection of AβO, using molecularly imprinted polymers (MIPs) and aptamer as the recognition element. Instead of using an antibody to recognize the AβO target molecules, the AβO in the samples were captured by the film of MIPs and the AβO-specific aptamer, forming a MIPs/target/aptamer sandwich assay for the highly selective detection of AβO. The AβO-specific aptamer was immobilized on the surface of core-shell nanoparticles that combined silver nanoparticles with silica nanoparticles (SiO$_2$@Ag NPs). The highly sensitive electrochemical signal from the sandwich assay was generated by using a small amount of AβO to trigger a large number of electrochemically active Ag NPs. Under the optimized conditions, the developed biosensor showed good linearity in the concentration range of 5 pg mL^{-1} to 10 ng mL^{-1} with a limit of detection of 1.22 pg mL^{-1}. The biosensor also showed excellent specificity, reproducibility and stability. In addition, the feasibility of detecting AβO in human serum was successfully verified, demonstrating the promising potential of this approach for clinical research and the early diagnosis of AD.

© 2020 Elsevier B.V. All rights reserved.

1. Introduction

Alzheimer's disease (AD) is a progressive and fatal neurodegenerative disorder, which is an enormous public health challenge due to the rapid aging of the global population [1]. The number of AD patients worldwide is estimated to reach 131.5 million by 2050, and a recent report has estimated that the annual total cost of dementia care is very high and will increase to a trillion dollars a year [2]. Thus, the early diagnosis of AD is extremely important for preventing and curing AD-caused dementia and death worldwide. According to recent reports, soluble amyloid-β oligomers (AβOs), rather than Aβ fibrils or Aβ monomers, are the most neurotoxic species involved in Alzheimer's pathogenesis [3,4]. AβOs are derived from the proteolytic cleavage of the amyloid precursor protein (APP) and obtained from Aβ peptides with lengths of 40–42 amino acids [5]. AβOs can then form the insoluble Aβ plaques that are the representative pathological feature of AD [6]. A variety of techniques have been used to detect AβOs [7], including electrochemistry [8,48,49], surface-enhanced Raman spectroscopy (SERS) [9], fluorescence [3], localized surface plasmon resonance (LSPR) [10,45], and mass spectrometry [11]. Although these methods have low limits of detection, they also have some inherent drawbacks, since they can be labor intensive and requiring complicated

instruments and expensive antibodies. Therefore, simple, low cost, sensitive and selective methods for the early diagnosis of AD are highly desirable.

In general, AβOs can be recognized and captured by antibodies or single-chain antibody fragments [12,13]. Alternatively, molecularly imprinted polymers (MIPs) can be used as synthetic antibody mimics for specific molecular recognition, and offer the advantages of high selectivity, chemical stability, easy tailoring, resistance to harsh environments, and potential applicability to all proteins [14,15]. The template used for the synthesis of MIPs can be the target molecule or a derivative of the target molecule [16,17]. The binding sites in the imprinted cavities of MIPs bind the target molecule with excellent affinity and selectivity [18], equivalent to the performance of natural antibodies [19]. These "artificial antibodies" have received significant interest and have yielded excellent results in many applications, including separation, biosensors, catalysis, and drug delivery [16,20–22]. Furthermore, MIPs have the potential for extensive application in biosensing and biomarker detection.

Recently, aptamers have been considered as potential alternatives to antibodies due to their impressive recognition features and their competitive advantages [23], including easy preparation, design versatility, facile modification, low molecular weight, simple structure, and chemical stability [24]. In addition, aptamers generally have high binding affinity and high selectivity for their specific target, including metal ions [25], amino acids [26], other small organic molecules [27,28], viral proteins [29–31], and

* Corresponding author.
E-mail address: fzhang@chem.ecnu.edu.cn. (F. Zhang).

even entire cells [32]. Aptamers have been widely employed in the fields of diagnostics, therapeutics, molecular imaging, and biosensors [33–35]. In particular, biosensors based on aptamers exhibit extraordinary advantages compared with biosensors that use natural antibodies or enzymes as receptors [36]. Fortunately, Tsukakoshi's group has obtained an AβO-specific aptamer using a competitive screening method based on aptamer blotting [37], which can potentially be applied in diagnostic assays for AD.

In this study, a highly sensitive and selective electrochemical biosensor was reported for the detection of AβO using MIPs and aptamer to recognize AβO. As shown in Scheme 1A, core-shell nanoparticles that combine silver nanoparticles with silica nanoparticles ($SiO_2@Ag$) were introduced to generate and amplify the electrochemical signal. The AβO-specific aptamer was assembled on the surface of the $SiO_2@Ag$ nanoparticles using a Ag-SH bond, forming a $SiO_2@Ag$-aptamer bioconjugate. The molecularly imprinted substrates were fabricated using a glassy carbon electrode (GCE), which was first coated with a gold nanoparticle and reduced graphene oxide (AuNPs-GO) composite, followed by a molecularly imprinted layer in the presence of the AβO template (Scheme 1B). GO and AuNPs were used to improve the electrical conductivity and the surface-to-volume ratio due to their good conductivity and high surface area [35]. The AβO in samples were then specifically captured by the MIPs film, which acted as an artificial antibody. After removing nonspecifically bound species, the captured targets bound to the $SiO_2@Ag$-aptamer, producing electrochemical signals due to the formation of a sandwich structure on the MIPs film. This sandwich assay electrochemical biosensor showed high specificity and sensitivity towards AβO, with a limit of detection (LOD) of 1.22 pg mL^{-1} (S/N = 3), which is similar to the concentration of AβOs in AD patients [4,8]. Additionally, this approach showed promising results in the determination of AβOs.

2. Experimental

2.1. Chemicals and reagents

Silver nitrate ($AgNO_3$), $NH_3 \cdot H_2O$, chloroauric acid ($HAuCl_4 \cdot 4H_2O$), sodium borohydride ($NaBH_4$), graphite powder (analytical grade), chitosan, L-ascorbic acid (AA), trisodium citrate, methanol (MeOH), ethanol, anhydrous acetonitrile, n-hexanol, cyclohexane, dimethyl sulfoxide (DMSO), tetraethoxysilane (TEOS), Triton X-100, N,N'-methylenebis(acrylamide) (MBA), methacrylic acid (MAA), and methacrylamide (MAC) were all purchased from Sinopharm Chemical Reagent (Shanghai, China). Tris(2-carboxyethyl)phosphine (TCEP), tetrabutylammonium hydroxide (TBA), 4-vinylpyridine (4-VPY), divinylbenzene (DVB), 1,1,1,3,3,3-hexafluoro-2-propanol (HFIP), polyvinylpyrrolidone (PVP, MW = 55,000), and N-(3-Aminopropyl)methacrylamide hydrochloride (APMAA) were provided by

Sigma-Aldrich (St. Louis, MO). N,N'-azo-bis-(2,4-dimethyl)valeronitrile (ABDV) and 1,3-diallylurea (DAU) were purchased from Tokyo Chemical Industry (TCI) Development Co., Ltd. (Shanghai, China). The AβO aptamer with the sequence 5′-HS-GCCTGTGGTGTTGGGGCGGGTGCG-3′ (HS-aptamer) was synthesized by Sangon Biotechnology Co., Ltd. (Shanghai, China) and purified using HPLC. Purified synthetic AβOs DAEFRHDSGYEVHHQKLVFFAEDVGSNKGAIIGLMVGGVV (Aβ$_{1-40}$) and DAEFRHDSGYEVHHQKLVFFAEDVGSNKGAIIGLMVGGVVIA (Aβ$_{1-42}$) (97 wt%) were obtained from ChinaPeptides Co. Ltd. (Shanghai, China). MAA was distilled under reduced pressure to remove the polymerization inhibitor. Other chemicals and reagents were used as received without further purification. Clinical human serum samples were collected from a local pathology laboratory and stored at 4 °C. Ultrapure water was obtained from a Hitech laboratory water purification system (≥ 18 MΩ·cm) and was used throughout the experiments. Phosphate buffer saline (PBS, 0.1 M, pH = 7.4) was prepared with ultrapure water and employed as the supporting electrolyte.

2.2. Instrumentation

Transmission electron microscopy (TEM) was performed using a JEOL JEM-2100F. The surface morphology was assessed using a HITACHI S-4800 scanning electronic microscope (SEM, Hitachi Co. Ltd., Tokyo, Japan). X-ray photoelectron spectroscopy (XPS) was performed using an ESCALAB 250, Thermo Fisher. The hydrodynamic sizes of the nanoparticles were determined by dynamic light scattering (DLS) using a Malvern Zetasizer instrument. Atomic force microscopy (AFM) was performed using a Veeco Nanoscope IIIa MultiMode AFM microscope in tapping mode. Fourier transform infrared (FT-IR) spectroscopy was performed using a NEXUS 670 FT-IR spectrometer (Nicolet, USA). UV–visible (UV–vis) absorption spectra were recorded with a UV-1800 spectrophotometer (Shimadzu, Japan). All of the electrochemical measurements were carried out using a CHI 820B electrochemical workstation (Shanghai Chenhua Instrument Corporation, China) at room temperature. A three-electrode system, which consisted of a modified glassy carbon electrode (GCE, 3 mm in diameter, working electrode), a platinum wire (auxiliary electrode), and a Ag/AgCl electrode with a saturated KCl solution (the reference electrode), for used in all the electrochemical investigations in a 10 mL glass cell.

2.3. Preparation of Aβ oligomers and fibrils

To prepare Aβ monomers, the obtained Aβ peptide powder was dissolved in HFIP at a concentration of 2 mg ml^{-1}, followed by overnight incubation at room temperature according to the previous work [3,50]. After evaporation of the HFIP using N_2 gas, the Aβ monomers were
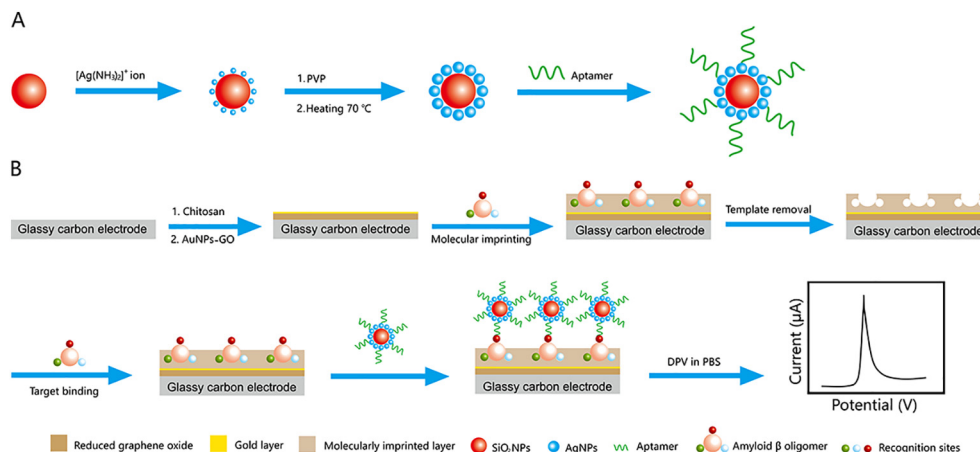
Scheme 1. Schematic illustration of (A) the preparation of the $SiO_2@Ag$-aptamer composite, and (B) the fabrication of the MIPs-based antibody-free biosensor and the electrochemical detection of AβO via a sandwich-type assay.

redissolved in DMSO and the obtained Aβ monomer solution (2 mg ml^{-1}) was stored at -20 °C for further use. The Aβ oligomers and fibrils were obtained by incubating a solution of Aβ monomers (1 mg ml^{-1}) in 10 mM Tris-HCl (pH = 7.4) with shaking at 37 °C in the dark for 10 h and 48 h, respectively.

2.4. Preparation of the SiO$_2$@Ag-aptamer bioconjugate

The SiO$_2$@Ag-aptamer bioconjugate was prepared according to the previously described procedure with some modifications [38]. First, SiO$_2$@Ag nanoparticles were synthesized according to the previously published procedure [38]. Then, the SiO$_2$@Ag nanoparticles were modified using HS-aptamer via AgS bond, yielding the SiO$_2$@Ag-aptamer bioconjugate. After that, 1 mg of the obtained SiO$_2$@Ag nanoparticles were resuspended in 1 mL of a 5 μM HS-aptamer solution, which had been previously activated using TCEP (10 mM). After continuous shaking at 37 °C for 12 h, the resulting SiO$_2$@Ag-aptamer composite was collected by centrifugation (10,000 rpm, 10 min), and washed with ultrapure water twice at room temperature. Finally, the products were suspended in 1.0 mL of 0.1 M PBS and stored at 4 °C until use.

2.5. Fabrication of the MIPs biosensor

The AuNPs-GO composite was prepared according to the previously published procedure with some modifications [39]. A bare GCE was first polished with alumina slurry and washed with ultrapure water under ultrasonication for 5 min. Then, 5 μL of a 1% chitosan solution and 5 μL of a 1.0 mg mL^{-1} AuNPs-GO solution were sequentially dropped onto the pretreated GCE and dried in air for 1 h (Scheme 1). To form the MIPs film, 5 μL of a polymer precursor solution, containing 1 mg mL^{-1} Aβ$_{1-42}$ oligomer, 2.0 mM MAA, 1 mM DAU, 1.25 mM DVB and 5 mM ABDV dissolved in a DMSO-acetonitrile solution (2:3, v/v), was coated on the modified GCE electrodes at room temperature. After heating at 50 °C for 12 h, the resulting electrodes were sequentially washed with MeOH, MeOH/ 0.1 M HCl (9:1, v/v), and MeOH until the current response of the electrode reached a constant value. As a control, electrodes modified with non-imprinted polymers (NIPs) were prepared using the same procedures as for the MIPs electrodes, but without using the template during the polymerization.

2.6. Electrochemical measurements

Prior to the measurements, the modified electrodes were first exposed to 5 μL of AβO at various concentrations in PBS buffer (0.1 M, pH 7.4) at 37 °C for 30 min in a humidity chamber. Then, 5 μL of the SiO$_2$@Ag-aptamer complex (1 mg mL^{-1}) was added to the electrode surface and incubated for 10 min at 37 °C. After rinsing with 0.1 M PBS (pH 7.4) for 10 min to remove any unbound SiO$_2$@Ag-aptamer, the electrodes were dried at room temperature. The electrochemical measurements were performed using differential pulse voltammetry (DPV) in the range of -0.2 V to $+0.6$ V with a pulse amplitude of 50 mV, a pulse period of 0.2 s and a pulse width of 50 ms.

3. Results and discussion

3.1. Characterization of SiO$_2$@Ag-aptamer

The AβO-specific aptamer self-assembled on the surface of SiO$_2$@Ag, enabling SiO$_2$@Ag-aptamer to bind with AβO and generate strong electrochemical signals. The monodispersed SiO$_2$@Ag could be clearly visualized by SEM and TEM (Fig. 1A–C). The average diameter of the SiO$_2$ NPs was around 200 nm and they had a uniform size distributions and smooth surfaces (Figs. 1A, S1A). While, SiO$_2$@Ag had many Ag NPs scattered on the surface with a uniform diameter of about 220 nm (Figs. 1B–C, S1B), indicating the successful synthesis of SiO$_2$@Ag. The dark-field scanning TEM image (Fig. 1D) and corresponding elemental maps of Si, O, and Ag

demonstrated the homogeneous distribution of Ag on the SiO$_2$ NPs. The energy dispersive spectrometer (EDS) spectra also showed the coexistence of the Si, O, and Ag signals, which also demonstrated the homogeneous distribution of Ag on the SiO$_2$ NPs (Fig. 1E). XPS was utilized to analyze the surface chemical composition of SiO$_2$@Ag. As shown in Fig. S2A, the XPS spectrum showed peaks from Si 2p, Si 2s, C 1s, N 1s, O 1s, Ag 3d (Ag 3d$_{5/2}$, Ag 3d$_{3/2}$) and Ag 3p (Ag 3p$_{5/2}$, Ag 3p$_{3/2}$), which are strong evidence for the successful addition of elemental of Ag[40]. The presence of the nitrogen (N 1s) and carbon (C 1s) signals further confirmed the presence of PVP on the SiO$_2$@Ag surface (Fig. S2A–B). The O 1s peak, shown in Fig. S2C, could be deconvoluted into three peaks with binding energies of 532, 531.7, and 530.7 eV. The peak at 531.7 eV can be attributed both to the interaction between the oxygen in the carboxyl groups of PVP with the Ag NPs and to hydrogen bonding between PVP and SiO$_2$ [40]. As shown in Fig. S2D, the Ag 3d XPS spectrum of SiO$_2$@Ag could be fit with a typical Ag 3d doublet at 367.8 and 373.8 eV with a spin-orbit splitting of 6 eV, corresponding to the Ag 3d$_{5/2}$ and Ag 3d$_{3/2}$ binding energies, respectively [40]. These two Ag 3d$_{5/2}$ and Ag 3d$_{3/2}$ peaks (367.8 eV and 373.8 eV) of SiO$_2$@Ag were shifted to lower binging energies compared to pure Ag (368.2 eV for Ag 3d$_{5/2}$, 374.2 eV for Ag 3d$_{3/2}$), which further confirmed the interaction between the SiO$_2$ and Ag NPs.

Furthermore, the UV–vis spectrum of the thiol-labeled AβO-specific aptamer showed a characteristic peak at 260 nm (Fig. 1F curve a), due to the absorption of purine and thymine bases. The pure SiO$_2$ NPs did not display any peaks in the test window (Fig. 1F, curve b). After the addition of the Ag NPs, an obvious plasmon absorption peak near 420 nm was observed for SiO$_2$@Ag (Fig. 1F, curve c), which can be attributed to Mie plasmon resonance excitation induced by the Ag NPs. As the thiol-labeled AβO-specific aptamer was assembled on the surface of SiO$_2$@Ag via AgS bond, the SiO$_2$@Ag-aptamer bioconjugate exhibited two characteristic peaks at 260 nm and 420 nm (Fig. 1F, curve d). These results indicate that SiO$_2$@Ag-aptamer was successful prepared.

3.2. Characterization of the MIPs film

The FT-IR spectra of the MIPs with and without the template and of the NIPs were obtained to verify the removal of the peptide template from the MIPs film. As shown in Fig. 1G, the characteristic peaks at 1735 cm^{-1} and 1167 cm^{-1} were attributed to the CO and CO stretching vibrations [41], respectively, demonstrating that all three polymers contain carboxyl groups derived from MAA. In addition, the characteristic peaks at approximately 3030 cm^{-1} and 900 cm^{-1} corresponded to the CH and CC stretching of the benzene ring, which indicated the presence of DVB in the three polymers. The bands at 3414 cm^{-1} and 1509 cm^{-1} in the spectrum of the MIPs with the template were assigned to the NH stretching vibration of the peptide template [41]. These two bands were relatively weak in the spectra of the NIPs and of the MIPs without the template. These results suggested that the imprinting and the subsequent extraction of the peptide template were successful.

In addition, AFM was used to identify the surface topography of the NIPs and MIPs in a 0.5 × 0.5 μm^2 scanned area. As shown in Fig. 2, the surface of the NIPs film displayed a relatively smooth morphology and some blocks that bulged (Fig. 2A). In contrast, the surface of the MIPs film showed many imprinted cavities (Fig. 2B). These results confirm the successful fabrication of the MIPs film.

3.3. Electrochemical behaviors of the MIPs biosensor

The electrochemical behaviors of the MIPs film were investigated using cyclic voltammetry (CV) and electrochemical impedance spectroscopy (EIS). As shown in Fig. 3A, bare GCE showed the peaks of a reversible redox couple of peaks with a peak potential separation (ΔE_p) of approximately 100 mV (Fig. 3A, curve a). The current intensity of AuNPs-GO/ GCE increased compared to that of the bare electrode due to the excellent conductivity and larger surface area of AuNPs-GO (Fig. 3A, curve b). After addition of the NIPs film, the modified electrode exhibited an obvious
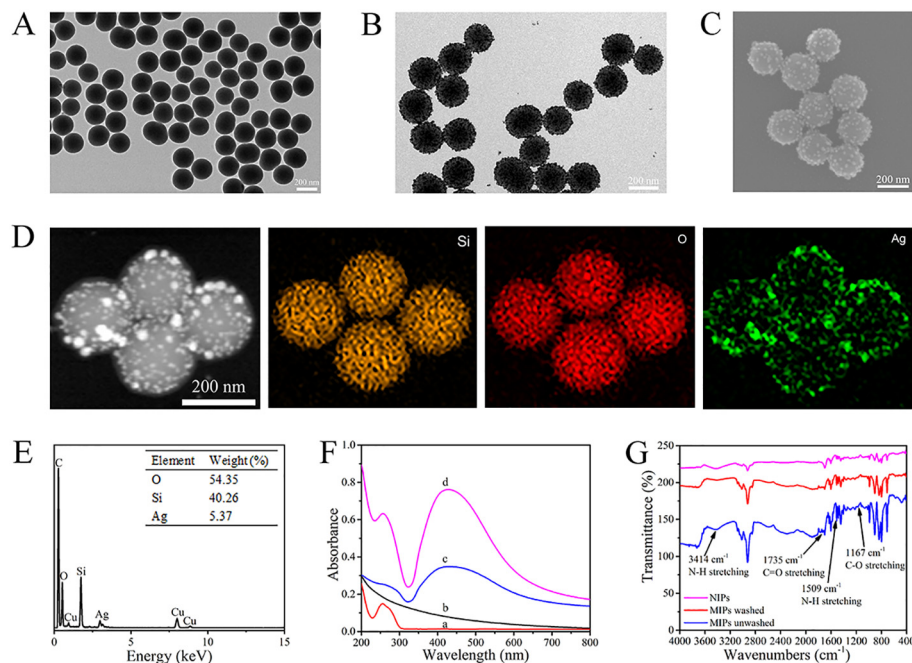
Fig. 1. (A) TEM image of the SiO$_2$ NPs. (B) TEM image, (C) SEM image, and (D) dark-field scanning TEM and corresponding elemental mapping images of SiO$_2$@Ag. (E) A representative EDS spectrum and data of SiO$_2$@Ag. (F) UV–vis spectra of the thiol-labeled aptamer (a), SiO$_2$ NPs (b), SiO$_2$@Ag (c), and SiO$_2$@Ag-aptamer (d). (G) FT-IR spectra of MIPs with and without the template and NIPs.

reduction in current intensity (Fig. 3A, curve c), demonstrating the large transfer resistance of the polymer film. When the electrode was coated with the MIPs film in the presence of the template, the Fe(CN)$_6^{3-/4-}$ redox peaks almost disappeared (Fig. 3A, curve d), suggesting an even greater electron transfer resistance. In contrast, after the template was removed from the MIPs film, the current increased significantly (Fig. 3A, curve e), because the three-dimensional (3D) imprinted cavities that were left in the MIPs film enhanced the Fe(CN)$_6^{3-/4-}$ diffusion and accelerated the electron transfer. Fig. 3B showed that the electrical properties of the biosensor could be fit using an equivalent circuit with four parameters, including the solution resistance (R$_s$), the charge transfer resistance between the electrode and the solution interface (R$_{et}$), the double layer capacitance of the electrodes (C$_{dl}$) and the Warburg impedance (W) [42]. R$_{et}$ was determined from the diameter of the semicircle of the Nyquist curve [42]. The EIS results in Fig. 3B are consistent with the CV results and both sets of

results indicate that the MIPs film were successfully fabricated on the electrodes surface and its electrical properties were improved by the imprinted cavities.

3.4. Optimization of the experimental conditions

To obtain the MIP film with the best performance, the key experimental parameters were optimized, including the type of monomer, the MAA to DAU ratio, the template concentrations, the AβO-specific aptamer concentration, the incubation time for the binding of the MIPs with AβO, and the washing time. Herein, six monomers, including MAA, DAU, MAC, MBA, APMAA, and 4-VPY, were considered (Fig. S3). Based on the characteristics of AβO and the results reported by Urraca et al. [43], MAA and DAU were used as monomers. The Aβ$_{1-42}$ oligomer molecule contains several amide groups and carboxyl groups [9], the carboxyl group in MAA binds with
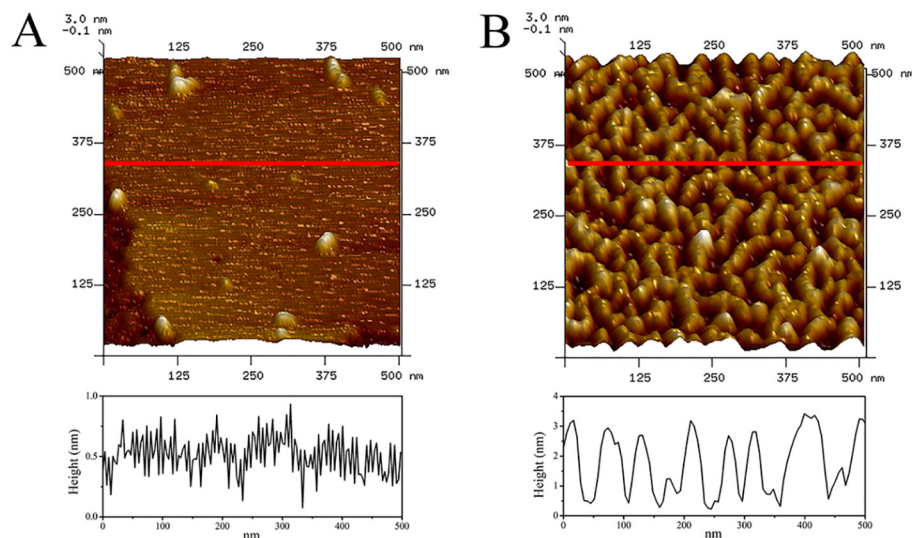
Fig. 2. AFM images of (A) the NIPs film and (B) the MIPs film after removal of the template, together with a cross-sectional profile across the indicated line.
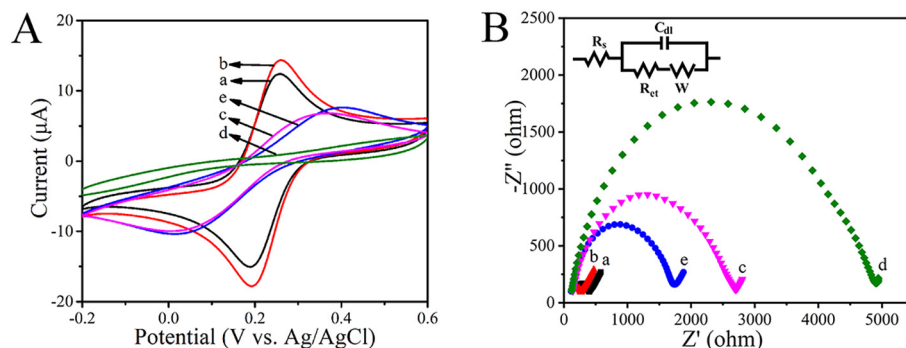
Fig. 3. (A) CV and (B) EIS of (a) bare GCE, (b) AuNPs-GO/GCE, (c) NIPs/AuNPs-GO/GCE, (d) MIPs/AuNPs-GO/GCE with the template, and (e) MIPs/AuNPs-GO/GCE after removal of the template, in a 5 mM $K_3[Fe(CN)_6]/K_4[Fe(CN)_6]$ solution containing 0.1 M KCl. Inset: the equivalent circuit obtained from the Nyquist plot.

amide group via hydrogen bond, and the amide groups in DAU interact with carboxyl groups through hydrogen bond and electrostatic interaction [43]. These binding sites effectively improve the binding effect of MIPs towards template due to a correct placement of complementary functional groups in the binding cavities and the microporous morphology of MIPs. MAC was tested due to its structural similarity to MAA, since its amino group could bond with a carboxyl group in AβO. MBA was employed because of its two amide groups, which could interact with the carboxyl group in AβO. APMAA contains a positively charged amino group and has the potential to strongly bind the AβO peptide. 4-VPY has a positively charged group and a pyridine ring, which form an electrostatic interaction with AβO. As shown in Fig. 4A, the current signals obtained for the MIPs with MAA and DAU were obviously stronger than those with other monomers. These can be attributing to the enhanced hydrogen bonding interaction with AβO due to the carboxyl groups of MAA, and the hydrogen bonding interactions and electrostatic interactions from the amide groups of DAU. The results show that the imprinted cavities in the MIPs provide enough strong binding sites with high affinity and selectivity for AβO. Hence, both MAA and DAU were chosen as monomers for the synthesis of MIPs.

The ratio between the two monomers was also optimized, since the ratio directly affects the 3D structure of the imprinted cavities and binding sites and thus the amount of AβO binding with the MIPs film. The

electrochemical signal clearly increased as the ratio of MAA to DAU decreased from 5:1 to 2:1 and then reached a maximum value at a ratio of 2:1 (Fig. 4B). Furthermore, the imprinting factor [44] (IF = I_{MIPs}/I_{NIPs}, where I_{MIPs} is the current value of the MIPs biosensor and I_{NIPs} is the current value of the NIPs biosensor) also reached a maximum value of 8.62 at a ratio of 2:1. Therefore, 2:1 was chosen as the optimal MAA to DAU ratio for obtaining the best performance from the MIPs biosensor.

During the preparation of the MIPs film, the concentration of the template directly determines the number of imprinted cavities and thus influences the amount of $A\beta_{1-42}$ oligomer binding to the MIPs film. As shown in Fig. 4C, with increasing $A\beta_{1-42}$ oligomer concentration, the current response first increased and then plateaued at 1 mg mL^{-1}. These results illustrate that the adsorption of the $A\beta_{1-42}$ oligomer on the MIPs film is enhanced by an increased amount of template, resulting in an increased current response. However, the adsorption of the $A\beta_{1-42}$ oligomer on the surface of the MIPs film and its dispersion in solution reach a kinetic balance at concentrations above 1 mg mL^{-1}. Hence, 1 mg mL^{-1} $A\beta_{1-42}$ oligomer was chosen as the optimal template concentration.

The amount of AβO-specific aptamer used for the AβO recognition has an important effect on the electrochemical signal of the MIPs biosensor. Therefore, the concentration of aptamer added to the $SiO_2@Ag$ surface was also optimized. Fig. 4D shows that the peak current increased when the AβO-specific aptamer concentration increased from 0.1 to 5 μM.
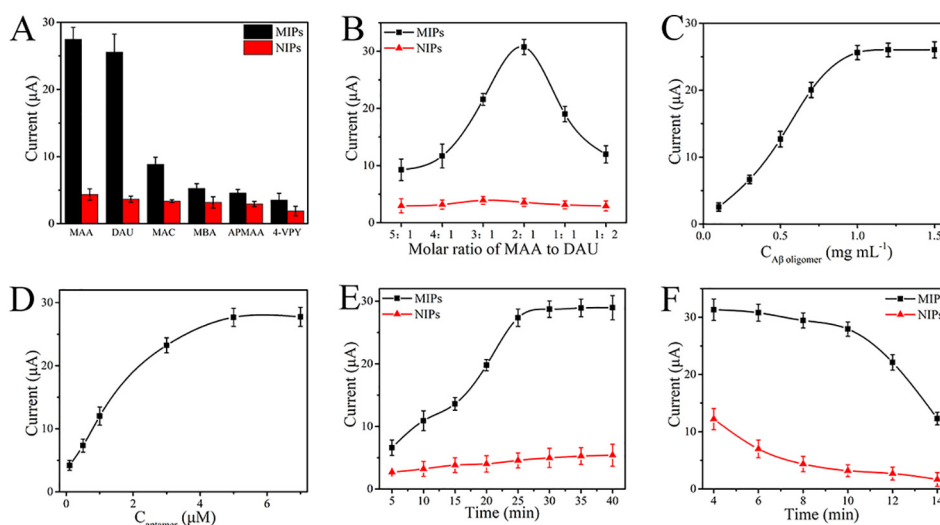
Fig. 4. (A) Current responses of 1 ng mL^{-1} $A\beta_{1-42}$ oligomer and MIPs/AuNPs-GO/GCE or NIPs/AuNPs-GO/GCE prepared with different functional monomers. (B) Effect of the molar ratio of MAA to DAU on the current response of MIPs/AuNPs-GO/GCE and NIPs/AuNPs-GO/GCE. (C) Current response of MIPs/AuNPs-GO/GCE prepared with different template concentrations ($C_{aptamer}$ = 10 μM aptamer). (D) Current response of MIPs/AuNPs-GO/GCE prepared with different aptamer concentrations ($C_{A\beta\ oligomer}$ = 1 ng mL^{-1}). (E) Effect of the incubation time for MIPs or NIPs binding with 1 ng mL^{-1} $A\beta_{1-42}$ oligomer. (F) Effect of the washing time for reducing the nonspecific adsorption in 1 ng mL^{-1} $A\beta_{1-42}$ oligomer.

However, the current response slightly decreased at the concentrations higher than 5 μM. These results suggest that the electron transfer in this electrochemical biosensor is inhibited by excess aptamer. Consequently, the optimal aptamer concentration was set at 5 μM for further studies.

The incubation time allowed for the AβO adsorption from solution by the imprinted cavities in MIPs film affected the amount of adsorbed AβO. As shown in Fig. 4E, the peak current of the MIPs biosensor obviously increased when the incubation time was increased from 5 to 30 min. However, when the time exceeded 30 min, the current response remained constant. The NIPs biosensor showed similar results. Moreover, the largest IF value of 5.78 was achieved after an incubation time of 30 min. Therefore, 30 min was chosen as the optimal incubation time.

Fig. 4F shows that the current responses of the MIPs and NIPs biosensors decreased as the washing time was increased from 4 to 14 min, suggesting that the elution process is unfavorable for polymer binding to AβO. Nevertheless, the elution process was necessary to obtain the highest IF value. Thus, 10 min was determined to be the optimal washing time.

3.5. Analytical performance of the MIPs biosensor

The DPV response of the prepared MIPs biosensor for AβO detection was recorded in 5 mL of a 0.1 M PBS solution (pH = 7.4) and compared with that of other modified electrodes. As the AuNPs-GO/GCE-MIP was rinsed with the AβO solution, AβO bound to the imprinted cavities on the surface of the MIPs film. Then the AβO bound in the MIPs film combined with SiO$_2$@Ag-aptamer via the specific binding between AβO and the aptamer. This resulted in the formation of a MIPs/target/SiO$_2$@Ag-aptamer sandwich structure. Finally, the response current increased due to AβO binding between the MIPs and the aptamer, because SiO$_2$ NPs with a large surface area could carry lots of electrochemically active Ag NPs and a large number of SiO$_2$@Ag were adsorbed on the surface of the electrode. Then this biosensor presented the amplification of the electrochemical signal, and microampere responses were achieved within the detection concentration range of the AβO. As indicated in Fig. 5A, a weak current response was obtained from AuNPs-GO/GCE, due to the weak adsorption of SiO$_2$@Ag-aptamer to AuNPs-GO (black line). Once the NIPs/AuNPs-GO were formed on the electrode surface, a slight increase in the oxidative peak was observed due to physical adsorption by the polymer (red line). After introducing MIPs/AuNPs-GO onto GCE, the current intensity without

rebinding of AβO (blue line) was stronger than that of NIPs/AuNPs-GO/GCE. This can be attributed to the adsorption of a small amount of SiO$_2$@Ag-aptamer onto the electrode surface by the 3D cavities in the MIPs film. When the MIPs/target/SiO$_2$@Ag-aptamer sandwich structure was completely formed, an obvious oxidative peak was obtained (pink line), demonstrating the successful construction of the biosensor, in which SiO$_2$@Ag significantly amplifies the electrochemical signal.

Aβ monomers, Aβ oligomers, and Aβ fibrils are all simultaneously present in the brain and in cerebrospinal fluid (CSF). However, AβOs are considered to be the most neurotoxic form in AD compared with Aβ fibrils and Aβ monomers. AβOs and Aβ fibrils can be formed by incubating Aβ monomers in 10 mM Tris-HCl (pH = 7.4) with shaking at 37 °C in the dark for 10 h and 48 h, respectively. The products were characterized by TEM (Fig. S4). Fig. 5B shows that the peak current intensities of the MIPs biosensor significantly increased as the Aβ$_{1-42}$ oligomer concentration increased from 5 pg mL^{-1} to 30 ng mL^{-1}. However, the peak current remained almost constant at concentrations higher than 30 ng mL^{-1}. The MIPs biosensor displayed stronger current signals and a higher adsorption rate than the NIPs biosensor at the same Aβ$_{1-42}$ oligomer concentration. This is due to the excellent specificity exhibited by the MIPs biosensor for the Aβ$_{1-42}$ oligomer in the detected concentration range, while the response of the NIPs biosensor is due to nonspecific adsorption of the target. In addition, an IF value of 9.1 was calculated for the MIPs biosensor at maximum binding concentrations of the MIPs and NIPs.

To further evaluate the specificity of the MIPs biosensor for the detection of Aβ oligomers, the responses towards Aβ$_{1-40}$ monomer, Aβ$_{1-42}$ monomer, Aβ$_{1-40}$ oligomer, Aβ$_{1-42}$ oligomer, Aβ$_{1-40}$ fibril, and Aβ$_{1-42}$ fibril were recorded under identical conditions. As shown in Fig. 5C, the current response of the Aβ monomers and Aβ fibrils were obviously weaker than that of the Aβ oligomers, due to the excellent specific recognition of Aβ oligomers by the MIPs film and the aptamer. In addition, similar intensities were observed for Aβ$_{1-40}$ oligomer and Aβ$_{1-42}$ oligomer. This can be attributed to the similar properties and 3D structure of the Aβ$_{1-40}$ oligomer and Aβ$_{1-42}$ oligomer, which only differ by two amino acids. Therefore, the prepared MIPs biosensor showed high specificity towards Aβ oligomers.

The sensitivity of this biosensor was investigated by detecting different concentrations of Aβ$_{1-42}$ oligomer under the optimized conditions. The electrochemical signal clearly increased as the Aβ$_{1-42}$ oligomer concentration increased (Fig. 5D). In addition, a strong linear correlation was
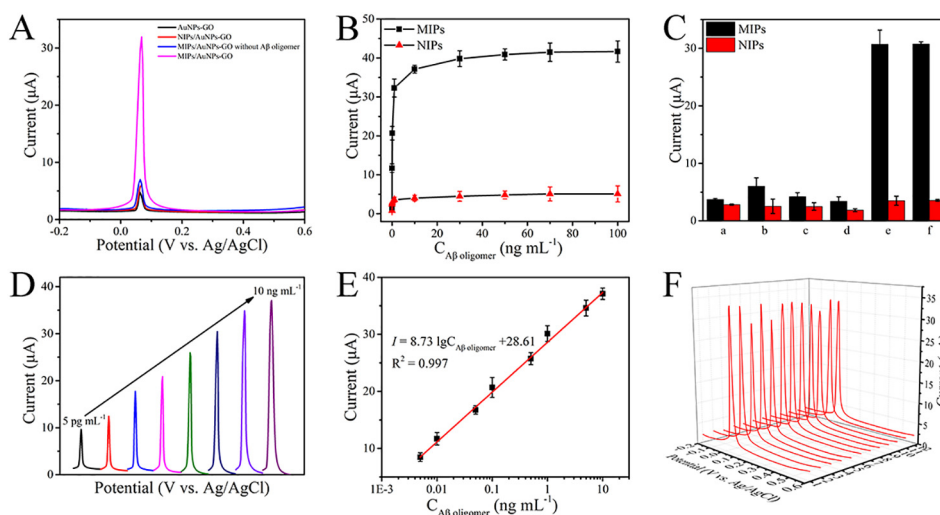
Fig. 5. (A) DPV responses obtained on the AuNPs-GO/GCE (black line), NIPs/AuNPs-GO/GCE (red line) and MIPs/AuNPs-GO/GCE (pink line) in 0.1 mM PBS (pH 7.4) after incubating with 1 ng mL^{-1} Aβ$_{1-42}$ oligomer for 30 min, and the DPV response obtained on MIPs/AuNPs-GO/GCE (blue line) in PBS without incubation. (B) Dependence of the peak current intensity detected by the MIPs and NIPs biosensors on the concentration of Aβ$_{1-42}$ oligomer. (C) Specificity of the MIPs biosensor in 0.1 M PBS (pH 7.4) containing 1 ng mL^{-1} Aβ: (a) Aβ$_{1-40}$ monomer, (b) Aβ$_{1-42}$ monomer, (c) Aβ$_{1-40}$ fibril, (d) Aβ$_{1-42}$ fibril, (e) Aβ$_{1-40}$ oligomer, and (f) Aβ$_{1-42}$ oligomer. DPV curves of the MIPs biosensor (D) and calibration curve (E) in 0.1 M PBS (pH 7.4) for detecting Aβ$_{1-42}$ oligomer at different concentrations: 5 pg mL^{-1}, 10 pg mL^{-1}, 50 pg mL^{-1}, 100 pg mL^{-1}, 500 pg mL^{-1}, 1 ng mL^{-1}, 5 ng mL^{-1} and 10 ng mL^{-1}. (F) DPV curves of 1 ng mL^{-1} Aβ$_{1-42}$ oligomer detected by twelve MIPs biosensors.

observed between the peak current and the logarithm of the $A\beta_{1-42}$ oligomer concentration ranging from 5 pg mL^{-1} to 10 ng mL^{-1} (Fig. 5E). The regression equation obtained was I (μA) = 8.73 lg C$_{A\beta\ oligomer}$ + 28.61 (R^2 = 0.997) and the LOD for $A\beta_{1-42}$ oligomer was 1.22 pg mL^{-1} (S/N = 3, where S is the standard deviation of the blank signals, and N is the slope of the corresponding calibration curve). Thus, the detection range of this biosensor agrees very well with the physiological concentration of Aβ oligomers in patients [4], which has been reported to be in the range of 1.25–12.5 ng mL^{-1}. The analytical performance of the antibody-free electrochemical biosensor developed for detecting AβOs was compared to the results of previous studies. As listed in Table 1, various methods, including fluorescent assays, SERS, LSPR, enzyme-linked immunoassays (ELISA) [46], electrochemiluminescence (ECL) [47] and electrochemical assays, have been widely applied to determine AβOs. Compared to these previously reported methods, the prepared biosensor exhibits excellent analytical performance in AβO detection.

3.6. Reproducibility and stability

To investigate the reproducibility, twelve MIPs biosensors were prepared under the same conditions and were then used to detect 1 ng mL^{-1} $A\beta_{1-42}$ oligomer. The relative standard deviation (RSD) was 7.7%, demonstrating that the prepared biosensors show good reproducibility (Fig. 5F). Moreover, the stability of the biosensor was evaluated by measuring the electrochemical signals every 7 days after storage at 4 °C (Fig. S5). After 28 days, the signal intensity retained ~91.2% of its initial value, demonstrating the robust stability of the biosensor.

3.7. Application to human serum samples

To evaluate the practical performances of the prepared biosensor, the recovery of $A\beta_{1-42}$ oligomer with spiked concentrations of 0, 0.1, 0.5, 1.0, 3.0, and 5.0 ng mL^{-1} in 10 folds-diluted healthy human serum samples was determined. As shown in Table 2, the $A\beta_{1-42}$ oligomer recovery values ranged from 93% to 107.7% with acceptable RSD values, indicating that this MIPs biosensor can be applied to the determination of AβO in clinical samples.

4. Conclusions

This work reported the preparation of a novel sandwich assay biosensor for the specific detection of AβO, which employed MIPs and an aptamer as the recognition element and SiO$_2$@Ag for the electrochemical signal amplification. This biosensor design used MIPs and the aptamer to replace natural antibodies for AβO detection, which shows significant advantages, including its low cost, portability, and the simplicity of the sample pretreatment and instrumentation. Under the optimized conditions, this MIPs/target/SiO$_2$@Ag-aptamer sandwich-structure biosensor exhibited high specificity and sensitivity with a low LOD. In addition, this biosensing method can be extended to detect other protein biomarkers using the appropriate MIPs and aptamers, providing a new approach to the use of

Table 1
Comparison of the performances of different methods developed for AβOs detection.

Method	Linear range (ng mL^{-1})	Detection limit (ng mL^{-1})	Reference
Fluorescence	0–7.7 $\times$ 10^4	14.3	3
SERS	400–4.8 $\times$ 10^3	400	9
LSPR	4 $\times$ 10^{-3}–4 $\times$ 10^5	6 $\times$ 10^{-3}	45
ELISA	0.039–2.1 $\times$ 10^3	0.039	46
ECL	1 $\times$ 10^{-4}–50	1.4 $\times$ 10^{-5}	47
Electrochemistry	0.8–160	0.2	8
Electrochemistry	0.08–6	0.04	48
Electrochemistry	0.08–400	0.03	49
Electrochemistry	2–120	0.4	50
Electrochemistry	5 $\times$ 10^{-3}–10	1.22 $\times$ 10^{-3}	This work

Table 2
Detection of $A\beta_{1-42}$ oligomer in clinical human serum samples (n = 3) using the proposed biosensor.

Sample	Added (ng mL^{-1})	Found (ng mL^{-1})	Recovery (%)	RSD (%)
1	0	0.01	–	–
2	0.1	0.10	103.0	8.5
3	0.5	0.47	94.0	6.4
4	1.0	1.06	106.0	2.5
5	3.0	3.23	107.7	7.1
6	5.0	4.65	93.0	9.8

MIPs and aptamers as alternatives for antibodies in biomarker detection. Finally, this approach is valuable for the determination of AβO and the early diagnosis of AD, and its potential applications in biosensors and disease diagnostics can be expanded.

CRediT authorship contribution statement

Min You: Investigation, Data curation, Writing - original draft, Writing - review & editing. **Shuai Yang:** Methodology, Formal analysis. **Yu An:** Methodology, Formal analysis. **Fan Zhang:** Supervision, Conceptualization, Writing - review & editing. **Pingang He:** Supervision, Funding acquisition.

Declaration of competing interest

The authors declare that they have no known competing financial interests or personal relationships that could have appeared to influence the work reported in this paper.

Acknowledgments

Appendix A. Supplementary data

Supplementary data to this article can be found online at https://doi.org/10.1016/j.jelechem.2020.114017.

References

[1] A.s. Association, 2018 Alzheimer's disease facts and figures, Alzheimer's Dementia 14 (2018) 367–429.
[2] E. Pellegrini, L. Ballerini, M.V. Hernandez, F.M. Chappell, V. González-Castro, D. Anblagan, S. Danso, S. Munoz-Maniega, D. Job, C. Pernet, G. Mair, T.J. MacGillivray, E. Trucco, J.M. Wardlaw, Machine learning of neuroimaging for assisted diagnosis of cognitive impairment and dementia: a systematic review, Alzheimer's & Dementia: Diagnosis, Assessment & Disease Monitoring 10 (2018) 519–535.
[3] L. Zhu, J. Zhang, F. Wang, Y. Wang, L. Lu, C. Feng, Z. Xu, W. Zhang, Selective amyloid β oligomer assay based on abasic site-containing molecular beacon and enzyme-free amplification, Biosens. Bioelectron. 78 (2016) 206–212.
[4] I.W. Hamley, The amyloid beta peptide: a chemist's perspective. Role in Alzheimer's and fibrillization, Chem. Rev. 112 (2012) 5147–5192.
[5] F.M. LaFerla, K.N. Green, S. Oddo, Intracellular amyloid-β in Alzheimer's disease, Nat. Rev. Neurosci. 8 (2007) 499–509.
[6] Z. He, J.L. Guo, J.D. McBride, S. Narasimhan, H. Kim, L. Changolkar, B. Zhang, R.J. Gathagan, C. Yue, C. Dengler, A. Stieber, M. Nitla, D.A. Coulter, T. Abel, K.R. Brunden, J.Q. Trojanowski, V.M.Y. Lee, Amyloid-β plaques enhance Alzheimer's brain tau-seeded pathologies by facilitating neuritic plaque tau aggregation, Nat. Med. 24 (2018) 29–38.
[7] A. Kaushik, R.D. Jayant, S. Tiwari, A. Vashist, M. Nair, Nano-biosensors to detect beta-amyloid for Alzheimer's disease management, Biosens. Bioelectron. 80 (2016) 273–287.
[8] Y. Yu, L. Zhang, C. Li, X. Sun, D. Tang, G. Shi, A method for evaluating the level of soluble β-amyloid$_{(1-40/1-42)}$ in Alzheimer's disease based on the binding of gelsolin to β-amyloid peptides, Angew. Chem. Int. Ed. 53 (2014) 12832–12835.
[9] L. Guerrini, R. Arenal, B. Mannini, F. Chiti, R. Pini, P. Matteini, R.A. Alvarez-Puebla, SERS detection of amyloid oligomers on metallorganic-decorated plasmonic beads, ACS Appl. Mater. Interfaces 7 (2015) 9420–9428.
[10] A.J. Haes, W.P. Hall, L. Chang, W.L. Klein, R.P. Van Duyne, A localized surface plasmon resonance biosensor: first steps toward an assay for Alzheimer's disease, Nano Lett. 4 (2004) 1029–1034.

[11] J. Pannee, J. Gobom, L.M. Shaw, M. Korecka, E.E. Chambers, M. Lame, R. Jenkins, W. Mylott, M.C. Carrillo, I. Zegers, H. Zetterberg, K. Blennowa, E. Portelius, Round robin test on quantification of amyloid-β 1-42 in cerebrospinal fluid by mass spectrometry, Alzheimer's Dementia 12 (2016) 55–59.

[12] J.M. Perchiacca, A.R.A. Ladiwala, M. Bhattacharya, P.M. Tessier, Structure-based design of conformation- and sequence-specific antibodies against amyloid β, Proc. Natl. Acad. Sci. 109 (2012) 84–89.

[13] D. Frenkel, B. Solomon, I. Benhar, Modulation of Alzheimer's b-amyloid neurotoxicity by site-directed singlechain antibody, J. Neuroimmunol. 106 (2000) 23–31.

[14] R. Gui, H. Jin, H. Guo, Z. Wang, Recent advances and future prospects in molecularly imprinted polymers-based electrochemical biosensors, Biosens. Bioelectron. 100 (2018) 56–70.

[15] M. Yoshikawa, K. Tharpa, S.-O. Dima, Molecularly imprinted membranes: past, present, and future, Chem. Rev. 116 (2016) 11500–11528.

[16] Z. Bie, R. Xing, X. He, Y. Ma, Y. Chen, Z. Liu, Precision imprinting of glycopeptides for facile preparation of glycan-specific artificial antibodies, Anal. Chem. 90 (2018) 9845–9852.

[17] J. Liu, D. Yin, S. Wang, H.Y. Chen, Z. Liu, Probing low-copy-number proteins in a single living cell, Angew. Chem. Int. Ed. 55 (2016) 13215–13218.

[18] T. Takeuchi, H. Sunayama, Beyond natural antibodies - a new generation of synthetic antibodies created by post-imprinting modification of molecularly imprinted polymers, Chem. Commun. 54 (2018) 6243–6251.

[19] J. Pan, W. Chen, Y. Ma, G. Pan, Molecularly imprinted polymers as receptor mimics for selective cell recognition, Chem. Commun. 47 (2018) 5574–5587.

[20] R. Schirhagl, Bioapplications for molecularly imprinted polymers, Anal. Chem. 86 (2013) 250–261.

[21] F.T. Moreira, B.A. Rodriguez, R.A. Dutra, M.G.F. Sales, Redox probe-free readings of a β-amyloid-42 plastic antibody sensory material assembled on copper@carbon nanotubes, Sensors Actuators B Chem. 264 (2018) 1–9.

[22] M.L. Yola, N. Atar, A review: molecularly imprinted electrochemical sensors for determination of biomolecules/drug, Curr. Anal. Chem. 13 (2017) 13–17.

[23] J. Zhou, J. Rossi, Aptamers as targeted therapeutics: current potential and challenges, Nat. Rev. Drug Discov. 16 (2017) 181–202.

[24] W. Tan, M.J. Donovan, J. Jiang, Aptamers from cell-based selection for bioanalytical applications, Chem. Rev. 113 (2013) 2842–2862.

[25] C. Li, Y. Peng, H. Wang, A. Liang, Z. Jiang, A nanosol SERS method for quantitative analysis of trace potassium based on aptamer recognition and silver nanorod catalysis of Ag(I)-glucose reaction, Sensors Actuators B Chem. 281 (2019) 53–59.

[26] M. Famulok, Molecular recognition of amino acids by RNA-aptamers: an L-citrulline binding RNA motif and its evolution into an L-arginine binder, J. Am. Chem. Soc. 116 (1994) 1698–1706.

[27] L. Yang, H. Ni, C. Li, X. Zhang, K. Wen, Y. Ke, H. Yang, W. Shi, S. Zhang, J. Shen, Z. Wang, Development of a highly specific chemiluminescence aptasensor for sulfamethazine detection in milk based on in vitro selected aptamers, Sensors Actuators B Chem. 281 (2019) 801–811.

[28] H. Yu, J. Canoura, B. Guntupalli, O. Alkhamis, Y. Xiao, Sensitive detection of small-molecule targets using cooperative binding split aptamers and enzyme-assisted target recycling, Anal. Chem. 90 (2018) 1748–1758.

[29] H. Zhang, F. Li, B. Dever, X.-F. Li, X.C. Le, DNA-mediated homogeneous binding assays for nucleic acids and proteins, Chem. Rev. 113 (2012) 2812–2841.

[30] Y.-X. Chen, K.-J. Huang, L.-L. He, Y.-H. Wang, Tetrahedral DNA probe coupling with hybridization chain reaction for competitive thrombin aptasensor, Biosens. Bioelectron. 100 (2018) 274–281.

[31] Y.-H. Wang, Y.-X. Chen, X. Wu, K.-J. Huang, Electrochemical biosensor based on Se-doped MWCNTs-graphene and Y-shaped DNA-aided target-triggered amplification strategy, Colloids Surf. B: Biointerfaces 172 (2018) 407–413.

[32] D. Ou, D. Sun, Z. Liang, B. Chen, X. Lin, Z. Chen, A novel cytosensor for capture, detection and release of breast cancer cells based on metal organic framework PCN-224 and DNA tetrahedron linked dual-aptamer, Sensors Actuators B Chem. 285 (2019) 398–404.

[33] H.-M. Meng, H. Liu, H. Kuai, R. Peng, L. Mo, X.-B. Zhang, Aptamer-integrated DNA nanostructures for biosensing, bioimaging and cancer therapy, Chem. Soc. Rev. 45 (2016) 2583–2602.

[34] Y.-X. Chen, X. Wu, K.-J. Huang, A sandwich-type electrochemical biosensing platform for microRNA-21 detection using carbon sphere-MoS2 and catalyzed hairpin assembly for signal amplification, Sensors Actuators B Chem. 270 (2018) 179–186.

[35] H.-L. Shuai, X. Wu, K.-J. Huang, Z.-B. Zhai, Ultrasensitive electrochemical biosensing platform based on spherical silicon dioxide/molybdenum selenide nanohybrids and triggered hybridization chain reaction, Biosens. Bioelectron. 94 (2017) 616–625.

[36] R. Ma, J. Liu, M.M. Ali, M.A.I. Mahmood, L. Labanieh, M. Lu, S.M. Iqbal, Q. Zhang, W. Zhao, Y. Wan, Nucleic acid aptamers in cancer research, diagnosis and therapy, Chem. Soc. Rev. 44 (2015) 1240–1256.

[37] K. Tsukakoshi, K. Abe, K. Sode, K. Ikebukuro, Selection of DNA aptamers that recognize α-synuclein oligomers using a competitive screening method, Anal. Chem. 84 (2012) 5542–5547.

[38] M. You, S. Yang, W. Tang, F. Zhang, P. He, Molecularly imprinted polymers based electrochemical DNA biosensor for the determination of BRCA-1 amplified by SiO2@Ag, Biosens. Bioelectron. 112 (2018) 72–78.

[39] J. Han, Y. Zhuo, Y.-Q. Chai, Y.-L. Yuan, R. Yuan, Novel electrochemical catalysis as signal amplified strategy for label-free detection of neuron-specific enolase, Biosens. Bioelectron. 31 (2012) 399–405.

[40] Z. Deng, M. Chen, L. Wu, Novel method to fabricate SiO2/Ag composite spheres and their catalytic, surface-enhanced Raman scattering properties, J. Phys. Chem. C 111 (2007) 11692–11698.

[41] L. Liu, T. Zhong, Q. Xu, Y. Chen, Efficient molecular imprinting strategy for quantitative targeted proteomics of human transferrin receptor in depleted human serum, Anal. Chem. 87 (2015) 10910–10919.

[42] Y. An, T. Jin, Y. Zhu, F. Zhang, P. He, An ultrasensitive electrochemical aptasensor for the determination of tumor exosomes based on click chemistry, Biosens. Bioelectron. 142 (2019), 111503.

[43] J.L. Urraca, C.S. Aureliano, E. Schillinger, H. Esselmann, J. Wiltfang, B.r. Sellergren, Polymeric complements to the Alzheimer's disease biomarker β-amyloid isoforms Aβ1-40 and Aβ1-42 for blood serum analysis under denaturing conditions, J. Am. Chem. Soc. 133 (2011) 9220–9223.

[44] J. Luo, Q. Ma, W. Wei, Y. Zhu, R. Liu, X. Liu, Synthesis of water-dispersible molecularly imprinted electroactive nanoparticles for the sensitive and selective paracetamol detection, ACS Appl. Mater. Interfaces 8 (2016) 21028–21038.

[45] M.K. Kang, J. Lee, A.H. Nguyen, S.J. Sim, Label-free detection of ApoE4-mediated β-amyloid aggregation on single nanoparticle uncovering Alzheimer's disease, Biosens. Bioelectron. 72 (2015) 197–204.

[46] T. Yang, S. Hong, T. O'Malley, R.A. Sperling, D.M. Walsh, D.J. Selkoe, New ELISAs with high specificity for soluble oligomers of amyloid β-protein detect natural Aβ oligomers in human brain but not CSF, Alzheimer's Dementia 9 (2013) 99–112.

[47] G. Zhao, Y. Wang, X. Li, Q. Yue, X. Dong, B. Du, W. Cao, Q. Wei, Dual-quenching electrochemiluminescence strategy based on three-dimensional metal-organic frameworks for ultrasensitive detection of amyloid-β, Anal. Chem. 91 (2019) 1989–1996.

[48] L. Liu, F. Zhao, F. Ma, L. Zhang, S. Yang, N. Xia, Electrochemical detection of β-amyloid peptides on electrode covered with N-terminus-specific antibody based on electrocatalytic O2 reduction by Aβ(1–16)-heme-modified gold nanoparticles, Biosens. Bioelectron. 49 (2013) 231–235.

[49] N. Xia, X. Wang, B. Zhou, Y. Wu, W. Mao, L. Liu, Electrochemical detection of amyloid-β oligomers based on the signal amplification of a network of silver nanoparticles, ACS Appl. Mater. Interfaces 8 (2016) 19303–19311.

[50] Y. Zhou, H. Zhang, L. Liu, C. Li, Z. Chang, X. Zhu, B. Ye, M. Xu, Fabrication of an antibody-aptamer sandwich assay for electrochemical evaluation of levels of β-amyloid oligomers, Sci. Rep. 6 (2016) 35.